Geothermal gradients and seismicity correlations in the Biga Peninsula (NW Türkiye) based on Curie point depths

Özcan Bektaş, Aydın Büyüksaraç, Eren Pamuk, Oktay Canbaz*

Abstract. The Biga Peninsula has hot springs with geothermal temperatures varying between 40°C and 175°C. In this study, we investigate the regional temperature distribution and change in radiogenic heat production in the Biga Peninsula. We use EMAG2 magnetic data to estimate the Curie point depth (CPD). Our findings show that the CPD in the region varies between 9 km and 17 km. We also calculated the geothermal gradient and heat flow values based on the CPD data. which range between 92.9 and 141.6 mWm^{-2}. Additionally, we also obtained values for z_o, z_t, and z_b from the power spectrum and calculated 1D geothermal gradient change for examined blocks. The resulting equations are: $z_t = z_{80°C}$, $z_o = z_{350°C}$, and $z_b = z_{580°C}$. These equations enabled us to propose a new formula to calculate the CPD. We also obtained the Conrad discontinuity depth ($z_c = z_{680°C}$) in the Biga Peninsula. Furthermore, we prepared 2D heat flow and temperature profiles along three sections to investigate the relationship between heat changes and earthquake focal distributions. The results indicate that seismicity is high in the southwest of the Biga Peninsula, which has a high CPD, high heat flow value, and shallow Conrad discontinuity.

Keywords: Biga Peninsula; Curie point depth; geothermal gradient; heat flow unit; Conrad discontinuity

✉ *Aydın Büyüksaraç* (absarac@comu.edu.tr),* ⦿ *https://orcid.org/0000-0002-4279-4158;*
Çanakkale Onsekiz Mart University, Çan Vocational School, TR-17400, Çanakkale, Türkiye
Özcan Bektaş
Sivas Cumhuriyet University, Department of Geophysical Engineering, TR-58140, Sivas, Türkiye;
Eren Pamuk
Erzincan Binali Yıldırım University, Institute of Earthquake Technologies, TR-24002 Erzincan, Türkiye;
Oktay Canbaz
Sivas Cumhuriyet University, Department of Geological Engineering, TR-58140, Sivas, Türkiye

*Corresponding author

INTRODUCTION

The Biga Peninsula (NW Türkiye), hosting the ancient city of Troy (Korfmann 2007), is situated between the North Anatolian Fault Zone (NAFZ) and the Region of Aegean Extension making it a tectonically active region (Şengör 1979; Şengör *et al*. 2005). The peninsula consists of various sedimentary, metamorphic, and igneous rocks of different ages (cf., Akbayram *et al*. 2016). Igneous rocks cover the largest area in the Biga Peninsula and are associated with geothermal systems and mineral deposits (Altunkaynak, Genç 2008; Çiçek, Oyman 2016).

In this study, we aimed to investigate the regional temperature distribution and changes in radiogenic heat production in the Biga Peninsula using the Global Earth Magnetic Anomaly Grid data (EMAG2) (Maus *et al*. 2008). Ekinci and Yiğitbaş (2012) presented the underground structures of the igneous rocks in the peninsula based on the analysis of magnetic anomalies. Hisarlı (1996) calculated the Curie depth calculation of the NW Aegean using aeromagnetic data. An inverse algorithm was developed for prism, dyke, and slope step models, and the heat gradient and heat flow values of the NW Aegean obtained using the Curie point depths (Marobhe 1989). According to

this shallow Curie point depths (between 6.5–8 km), high thermal gradients (75–85ºC/km) and a thin crust (~ 25 km, Ateş *et al.* 2012) were reported in the southern part of the Biga Peninsula (Marobhe 1989; Hisarlı 1996). In addition, deeper Curie point depths (> 10 km) were reported towards the southeast (in Balıkesir city) and west (Susurluk and Ilıca) of the peninsula, suggesting that the heat flow may be lower (< 60º C/km) in these regions (Hisarlı 1996). Studies based on spectral methods have become prominent in Curie depth calculation studies conducted in Türkiye. Most of these studies include calculations for specific regions in Türkiye (Table 1).

The presence of NE–SW directional right-lateral strike-slip and normal faults in the Biga Peninsula was obtained by Görgün and Albora (2017) through directional filter analysis applied to gravity anomalies. Their results are consistent with the aftershock orientation and the strikes of the Yenice-Gönen and Biga-Çan fault zones (Emre *et al.* 2013; Herece, Akay 2003; Şaroğlu *et al.* 1992), which are the most active fault zones in the peninsula. One branch of the NAFZ that extends into the Gulf of Saros is aligned in the same direction (Fig. 1). Data processing techniques applied to the derived gravity anomalies have been used to interpret the shallow structural features of the Biga and Gallipoli peninsulas (Ekinci, Yiğitbaş 2015). Derivative-based anomaly maps have revealed evidence of an ancient caldera structure in the western

part of the Biga Peninsula (Ekinci, Yiğitbaş 2015). In addition, sudden lateral changes in anomaly amplitudes have indicated the presence of significant structural discontinuities (Ekinci, Yiğitbaş 2015).

The compilation of studies presents significant advancements in understanding the Curie point depth (CPD), heat flow, geothermal characteristics and tectonic evolution of various regions through the application of magnetic anomaly analysis with EMAG2 data. Pamuk (2019) investigated CPDs and heat flow in Eastern Anatolia, employing edge detection methods to reveal correlations between subsurface geological features and geophysical parameters. Njeudjang *et al.* (2020) also estimated the CPD and geothermal gradients in the Adamawa volcanic region, highlighting the potential for geothermal energy exploitation in the area. In 2021, Yin *et al.* applied wavelet transforms to estimate the CPD, demonstrating the effectiveness of different methodologies in assessing geological structures, particularly in areas with varying heat flow rates. Mohamed and Deep (2021) utilized EGM2008 and EMAG2 data to develop a crustal thickness model for Africa, revealing a DBML depth ranging from 23.0 to 37.2 km and an average crustal thickness of 35.1 km. Heat flow varies widely across the continent, particularly reaching high values in the northern, eastern, and western regions, while geothermal gradients range from 14.5 to 23.6 °C/km. Harash and Chen (2022) explored the

Table 1 Curie point depth calculation studies conducted in Türkiye

Region	Geologic formation	CPD (km)	Reference
Central Anatolia	Volcanic Complex	7.9–22.6	Ateş *et al.* (2005)
	Galatian Volcanic Complex	6.7–17	Bilim (2011)
	Erciyes Volcano	13.7	Maden (2010)
	Yozgat Batholite	10.4–19.5	Bilim (2017)
	Cappadocia Volcanic Complex	7–12	Bilim *et al.* (2017a)
		7–22	Aydemir *et al.* (2019)
East Anatolia	Eastern Anatolian Volcanic Field	12.9–22.6	Bektaş *et al.* (2007)
	Inner East Anatolia	16.5–18.7	Bektaş (2013)
	Eastern part of the Anatolian plate and the Arabian Foreland	12–22	Elitok and Dolmaz (2008)
	Northern part of East Anatolia	15.7-18.6	Pamuk (2019)
	Eastern Anatolian Collisional Zone	12–14	Dolmaz *et al.* (2008)
West Anatolia	West Anatolian Extensional Province	6.5–11 10–20 8.2–19.9	Hisarlı (1996) Şalk *et al.* (2005) Dolmaz *et al.* (2005a)
	African-Eurasian convergence zone SW Anatolia south-eastern Aegean Sea and western part of Türkiye	9–20 9.8–19.5	Dolmaz *et al.* (2005b) Erbek and Dolmaz (2019)
	Menderes Massif and in the Aegean Region	6–12	Bilim *et al.* (2016)
	Bigadiç Basin and surroundings (NW Türkiye)	7–18	Bilim *et al.* (2021)
Thrace Region		9.7–20.3	Hisarli *et al.* (2012)
Black Sea	Pontides	14.3–27.9	Maden (2009)
	Eastern Black Sea basin and the eastern Pontides orogenic belt	25	Maden *et al.* (2013)
Mediterranean	Iskenderun Bay	8–13	Bilim *et al.* (2017b)
Whole Türkiye		6–10 in Eagean Region 20–29 Eastern Region	Aydın *et al.* (2005)
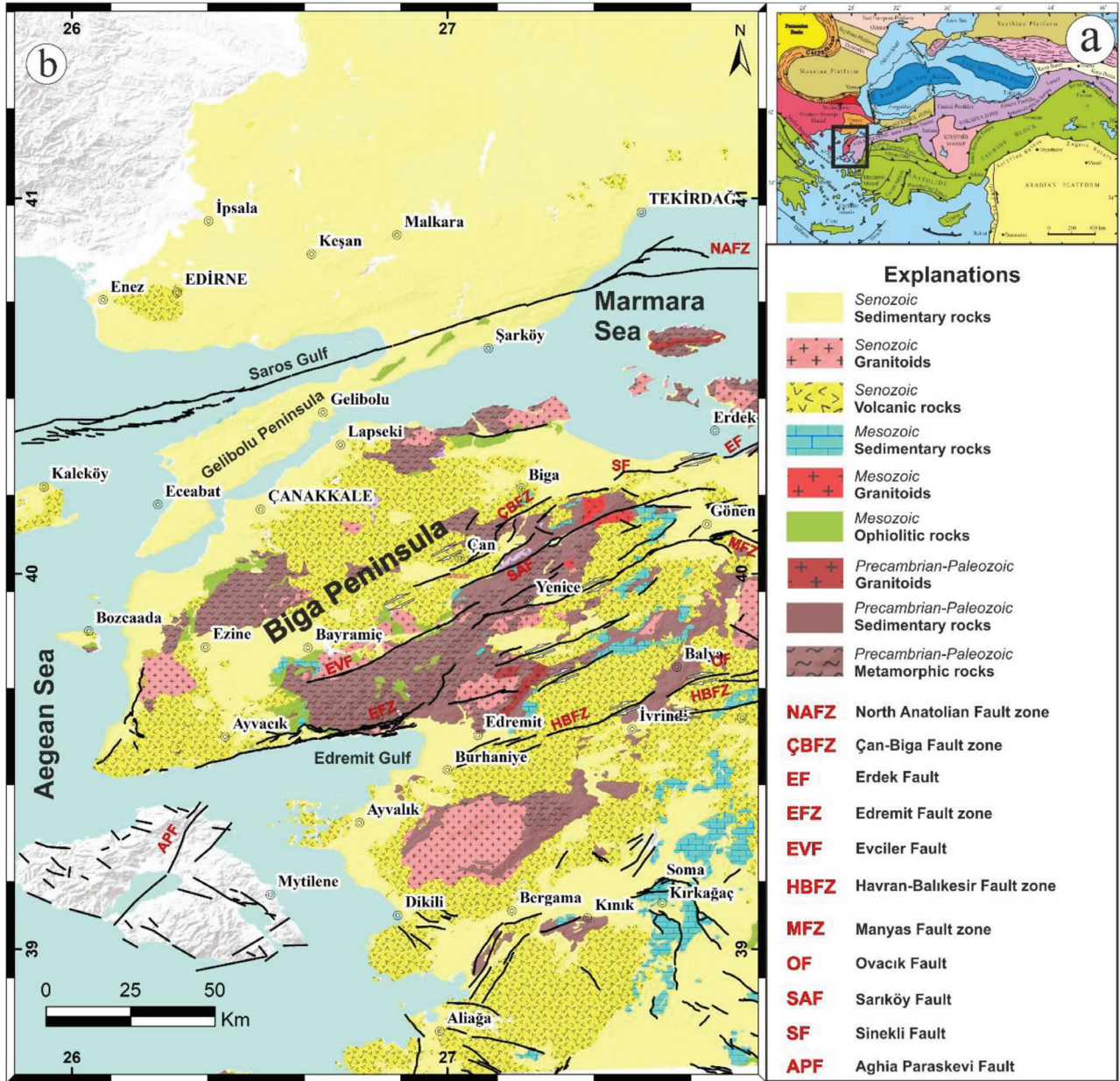
Fig. 1 a) The tectonic units of the Anatolian Peninsula, consisting of many continental pieces that came together in Late Tertiary to form a single landmass. Red rectangular shows the study area (Okay and Tüysüz 1999), **b)** Simplified geological map of the Biga Peninsula and active faults affecting the peninsula (Akbaş *et al*. 2011)

relationship between CPD and heat flow at the Eratosthenes Seamount, providing insights into thermal dynamics and the geothermal resource potential in the Eastern Mediterranean. Pamuk and Özsöz (2022) conducted a study on Cyprus Island, determining CPD and heat flow using EMAG2 data, identifying regions of high geothermal potential characterized by shallow CPD values. Njeudjang *et al*. (2023) provided a comprehensive database for the Adamawa region in Cameroon, focusing on heat flow, radiogenic heat production, and geothermal gradient, addressing energy challenges in sub-Saharan Africa. Jiao *et al*. (2025) analyzed the Eastern Himalayan Syntaxis, identifying a strong magnetic body indicative of deep material

uplift and supporting the "tectonic aneurysm" evolution model. These studies collectively contribute to a nuanced understanding of geothermal systems, crustal structures, and the potential for sustainable energy resources across diverse geological landscapes using EMAG2 data.

The main purpose of this study is to determine the variation in CPD by examining the magnetic anomalies of the Biga Peninsula and to model the temperature variation with depth. Throughout the study, approaches were developed to differentiate certain depths within the crust and identify key discontinuity levels. In particular, the fact that the Conrad discontinuity level obtained from the gravity data can also

17

be determined by temperature changes is significant in supporting other related studies. On the other hand, associating the focal depths of tectonic processes and earthquakes with heat models and defining these levels with specific heat values for the study area is presented as a new approach.

GEOLOGY AND TECTONICS

The Biga Peninsula is located in the north-western extremity of Türkiye and is bordered to the north by the Marmara Sea, to the south by the Edremit Gulf and to the southwest by the Aegean Sea (Fig. 1). Tectonically, the peninsula represents the westernmost extension of the Sakarya Zone of the Pontides (Eurasian plate) at the north of the İzmir–Ankara–Erzincan Suture Zone (IAESZ), which separates Gondwana (African and Arabian plates) from Laurasia (Eurasian plate) (Jankovic 1986; Okay *et al*. 1990, 1991; Okay, Tüysüz 1999; Sengör, Yilmaz 1981; Yiğit 2012). The collision of the Sakarya and the Anatolia-Tauride continent fragments that led to the closure of the Neo-Tethys Ocean resulted in a complex geological and tectonic structure of the region (Şengün *et al*. 2011; Yiğitbaş *et al*. 2009; Akbayram *et al*. 2016). Metamorphic, ophiolitic, igneous, and sedimentary rocks have widespread outcrops in the region (Dönmez *et al*. 2005; Duru *et al*. 2012, 2004). The Pre-Cenozoic metamorphic and ophiolitic rocks constitute the regional basement of the peninsula. Based on these units, the peninsula can tectonically be subdivided into four zones from northwest to southeast, which are the Gelibolu Zone, the Ezine Zone (Permian metasedimentary and Permo-Triassic ophiolitic rocks), the Ayvacık-Karabiga Zone (ophiolitic mélange bearing eclogite and Upper Cretaceous limestones blocks), and the Sakarya Zone (Permian metamorphics of Kazdağ Massif and Permo-Triassic metasedimentary rocks) (Okay *et al*. 1991). On the other hand, Yiğit (2012) proposes subdividing it into two zones from west to east: Rhodope-Strandja Zone and Sakarya Zone.

The Cenozoic igneous and sedimentary rocks cover a larger area than the metamorphic rocks and ophiolites in the Biga Peninsula (Gülyüz *et al*. 2020; Saatçi, Aslan 2018). Bozkaya *et al*. (2020) suggest four sub-time periods for these units: (1) Late Cretaceous-Early Eocene: basaltic lavas, turbiditic sandstones, and limestones (Delaloye, Bingöl 2000), (2) Middle Eocene-Oligocene: andesitic lavas and tuffs, granite, granodiorite and limestones (Krushensky 1976; Ayan 1979; Ercan, Türkecan 1984; Birkle, Satir 1995; Altunkaynak, Yılmaz 1999; Dönmez *et al*. 2005; Altunkaynak *et al*. 2012a; Yiğit 2012), (3) Miocene: granodiorite, rhyolitic and rhyodacitic pyroclastics, andesitic and dacitic lavas, and turbiditic clastics (Demirel *et al*. 2004; Altunkaynak *et al*.

2012b; Aslan *et al*. 2017), and (4) Plio-Quaternary: fluvial sediments and lacustrine carbonates.

The neotectonic period began with the interaction of the European, Arabian, and African plates and continues until today. During this period, two main fault zones, the NAFZ and the East Anatolian Fault Zone (EAFZ), formed as the active transform plate boundaries of Anatolian Plate. The NAFZ is divided into two branches in the Marmara region: the northern branch extending along the Saros Bay, and the southern branch extending along the Biga Peninsula (Barka, Kadinsky-Cade 1988; Siyako *et al*. 1989; Barka 1992). The southern branch of NAFZ is divided into three main branches in the Biga Peninsula, from the Middle Miocene to the present (Okay *et al*. 1991; Aldanmaz *et al*. 2000). The northern branch runs underneath the Marmara Sea, the middle branch continues across Ezine town, while the southern branch passes through the Edremit Graben (Aldanmaz *et al*. 2000). The sources of earthquakes affecting the Biga Peninsula include Saros Bay in the north, which is the western branch of the NAFZ, the Gönen-Yenice Fault Zone in the southwest-northeast direction, and the Edremit Bay and Ayvacık area in the south. Apart from this, significant earthquakes also occur in the Aegean Sea (Fig. 2). The largest earthquakes affecting this region include the 1912 Ganos (M = 7.2), the 1944 Edremit Bay (M = 6.8), the 1953 Yenice-Gönen (M = 7.2), and the 1983 Biga (M = 6.2) earthquakes.

To summarize, the peninsula is interacted by the dextral strike-slip NAFZ and the north-south extensional tectonic regime of the Aegean (McKenzie 1972, 1978; Taymaz *et al*. 1991). In addition, young magmatic rocks are widespread and exhibit a close spatial and temporal association with the faults (Karacık, Yılmaz 1998). Consequently, the Cenozoic magmatism and neotectonic activities have led to the development of the active faults where the geothermal resources are found (Fig. 2). Hot water resources in the Biga Peninsula were examined by many researchers. The temperatures of the geothermal resources vary between 35°C and 173°C in the peninsula. The Ayvacık-Tuzla geothermal spring has the highest temperature in this region, where geothermal energy is utilized (Koç *et al*. 2015). Although more than 50 hot water resources were identified, Demirel *et al*. (2004) marked 15 most known resources, and Deniz (2010) marked 19 on their maps. These resources are mostly concentrated around the fault zone extending NE–SW between Edremit Bay and Gönen in the east and south of the peninsula (Fig. 2). Recently, Wolkersdorfer *et al*. (2021) determined geothermal resources with temperatures ≥ 90° in the SE and NE parts of the area. These authors mapped new geothermal springs in the Biga Peninsula, especially around Troy.
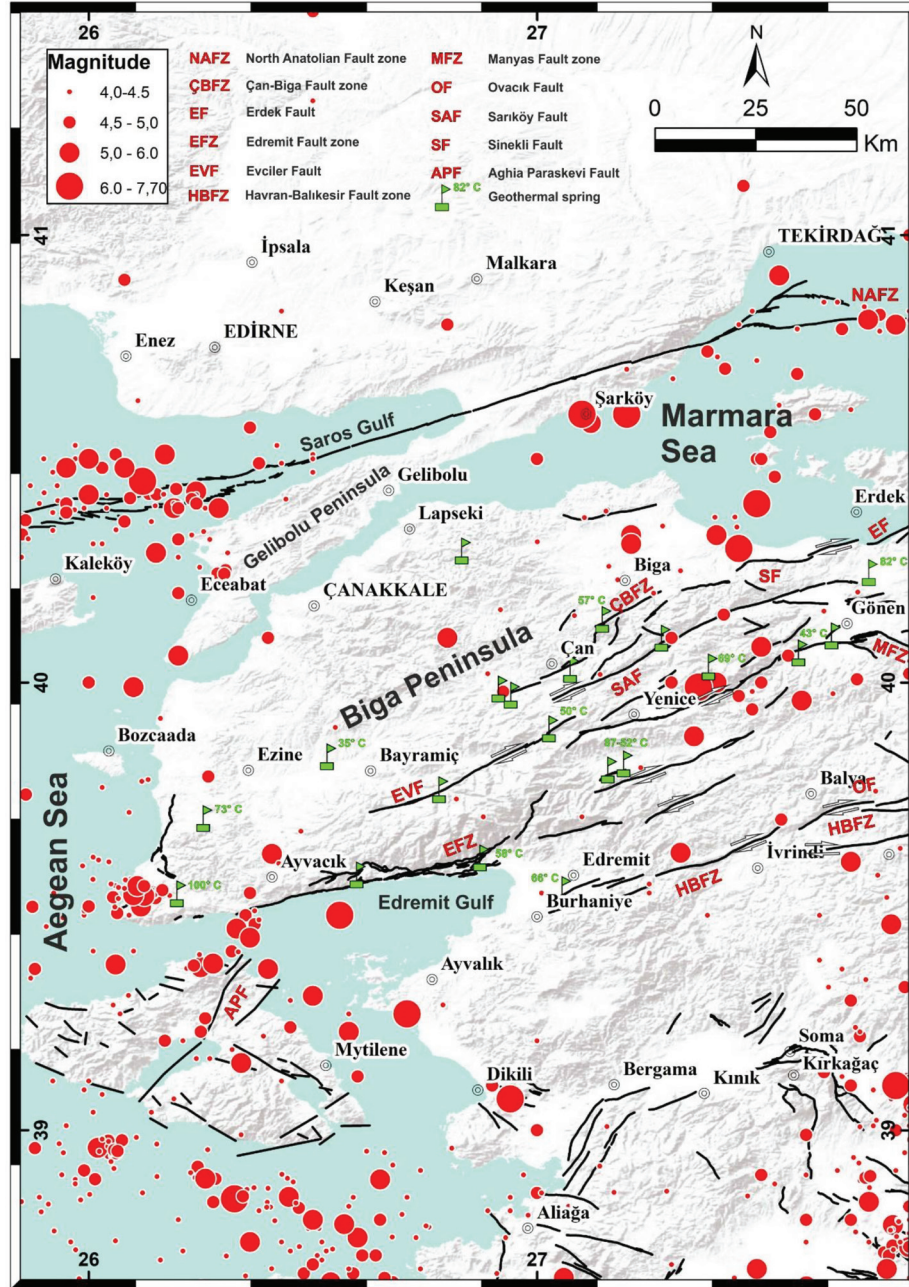
Fig. 2 The topographical map of the study area and its surroundings and the epicentral distribution of earthquakes (M ≥ 4.0) that affected the study area between 1900–2023

DATA AND METHODS

Magnetic data

The long wavelength data obtained above the CHAMP satellite with a height of 5 km from the ground according to the reference ellipsoid were evaluated and published as the Global Earth Magnetic Anomaly Grid (EMAG2) (Maus *et al.* 2008). In 2009, this altitude was reduced to 4 km with a resolution of 2 arc/min, and the third high-resolution version of EMAG2 was published. The EMAG2 magnetic data includes satellite, ship, and airborne measurements,

combining existing grids 4 km above the geoid with the least squares method. It also incorporates grids on the track lines using the anisotropic correlation function in the oceans, processing the magnetic data received in the air and at sea. This process includes the line levelling of the track line data, and satellite magnetic anomaly model was created with MF6 by substituting 120 degrees (330 km wavelength) spherical harmonic data (Maus *et al.* 2009). In this study, the EMAG2 magnetic data was used to calculate the Curie point depths (Fig. 3). To eliminate the aberrations caused by the geomagnetic field, the reduction-to-pole (RTP) transform was applied to the magnetic
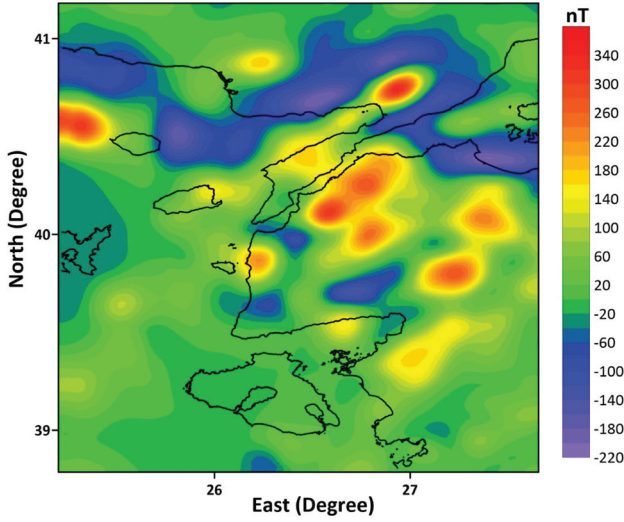
Fig. 3 Total field magnetic anomaly (TFMA) of the study area. EMAG2 data (downloaded from the National Oceanic and Atmospheric Administration (NOAA) geomagnetism database (https://www.ngdc.noaa.gov/geomag/emag2.html)
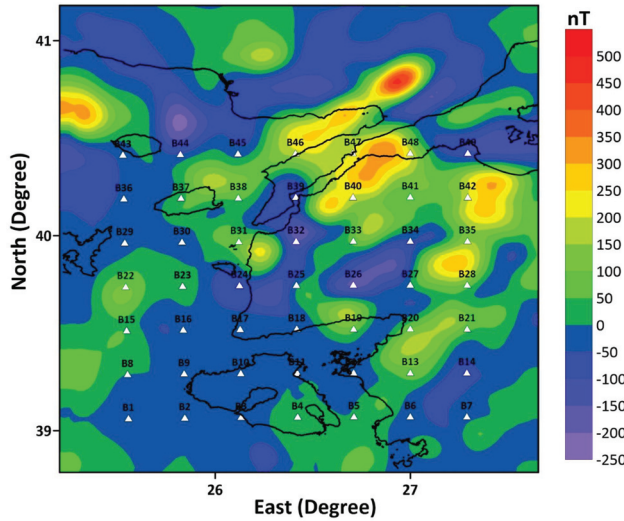
Fig. 4 Reduction-to-pole (RTP) magnetic anomaly map. The inclination and declination angles of the geomagnetic field and body magnetization accepted as 55° and 4°, respectively. The area is divided into 49 blocks of 50 km × 50 km on this map. Each block was created by overlaying the other by 50%. White triangles show the centres of the blocks and numbers used for the Curie point depth regions

anomalies shown in Fig. 3. During the RTP transform, the inclination and declination angles of the geomagnetic field and the angles of the object magnetization were assumed as 55° and 4°, respectively. The RTP magnetic anomaly map of the study area is given in Fig. 4.

Estimation of Curie point depth (CPD)

The Curie point depth (CPD) is known as the depth at which the magnetization level in the Earth's crust

changes from ferromagnetic to paramagnetic under the influence of increasing temperature (Nagata 1961; Dolmaz *et al.* 2005). This is the depth at which crustal temperatures reach the Curie point of the dominant magnetic minerals, possibly titanomagnetite with a Curie temperature of 580°C or lower (Nagata 1961). For this purpose, the base depth of the structure that causes magnetization from the magnetic data is considered the Curie point depth. CPD calculations have been developed progressively since the 1970s (Bhattacharyya, Leu 1975; Byerly, Stolt 1977; Shuey *et al.* 1977; Smith *et al.* 1974; Boler 1978; Connard *et al.* 1983; Okubo *et al.* 1985, 1989; Blakely 1988).

The methods used to determine the Curie point depths are based on spectral analysis. The simple two-dimensional spectral analysis technique of magnetic anomalies was first described by Spector and Grant (1970), and they stated that magnetic anomalies originate from vertical prisms. There are two basic methods for calculating the Curie point depth, both of which involve calculating the power spectrum. In this study, we calculated the Curie point depths of the Biga Peninsula by the power spectrum method developed by Okubo *et al.* (1985) and determined top (z_t), centre (z_o), and bottom (z_b) depths of the magnetic body. Okubo *et al.* (1985) stated that the spectrum can be written as Eq. 1 in polar coordinates in the frequency domain.

$$F(s,\psi) = 2\pi JA[N + 2(L\cos\psi + M\sin\psi)] \times$$
$$\times [n + i\ (1\cos\psi + \sin\psi)] \times \text{sinc}\ (\pi s\alpha\cos\psi)\ \text{sinc}\ (\pi sb\sin\psi)$$
$$\times \exp\ [-\ 2\pi si\ (xo\cos\psi + yo\sin\psi)]$$
$$\times [\exp\ (-2\pi szt) - \exp\ (-2\pi szb)], \tag{1}$$

where J is unit volume magnetization, A is the section of the body along one direction, L, M, N are direction cosines of the Earth magnetic field, a and b are the half-width and length of the source, i.e., half-width sizes along with the x and y directions, respectively, x_o and y_o are x and y centre coordinates of the object, and z_t and z_b are the top and bottom depths of the object.

Bhattacharyya and Leu (1975, 1977) and Okubo *et al.* (1985) suggested that the determination of the bottom depth (z_b) has two steps. The first step is the determination of the centre depth (z_o), and the second is the determination of the top depth (z_t). The bottom depth (z_b) obtained by using z_o and z_t depths is shown in Eq. 2.

$$Z_b = 2z_o - z_t \tag{2}$$

During the implementation of the method, we divided the RTP magnetic anomaly map (Fig. 4) into 49 blocks with a size of 50 km × 50 km. All of the blocks overlapped with adjacent blocks by 50 percent (25 km distance from each other). The centres of the blocks are marked with triangles (Fig. 4). The power spectrum method was then applied to 49 blocks in or-
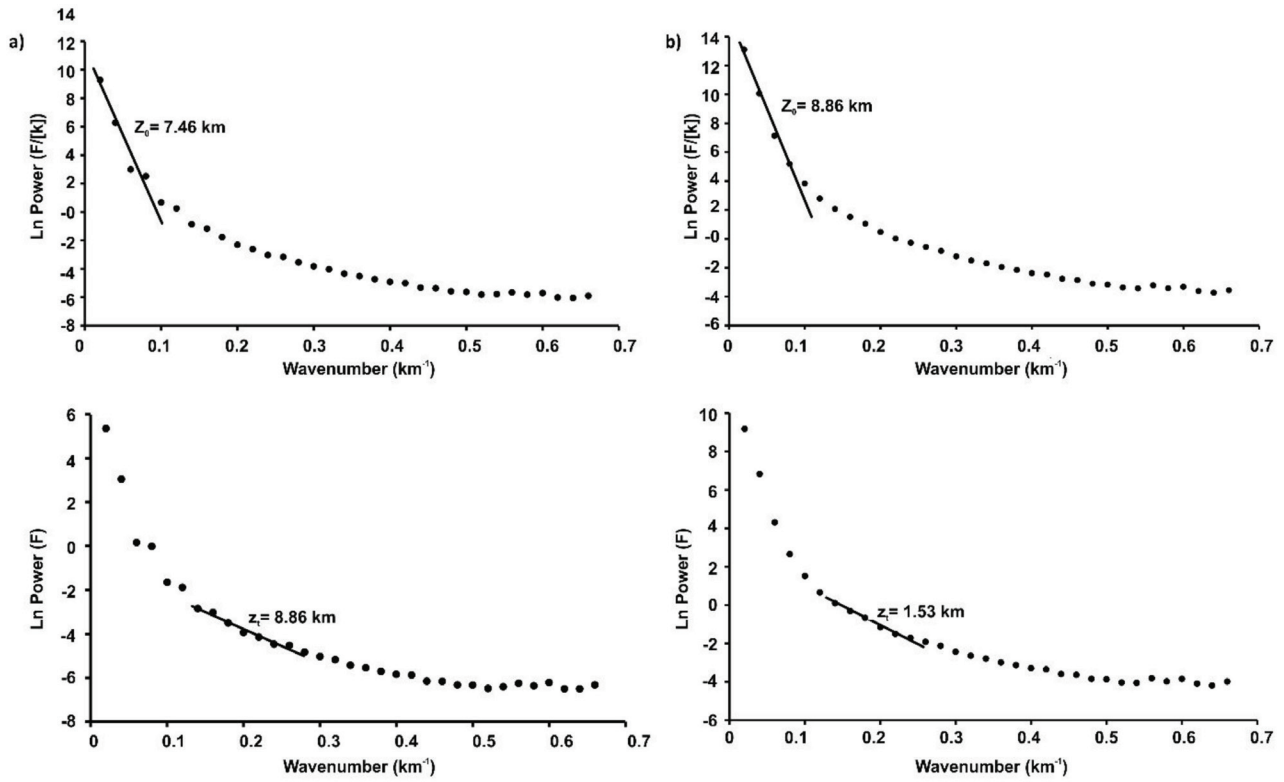
Fig. 5 Examples of the power spectrum analysis to estimate the depth to the base of magnetic sources (CPD): **a)** Representative Block-11, **b)** Representative Block-42. z_t is the depth of the top of the magnetic body, and z_o is the depth of the middle of the magnetic body

der to determine the Curie point depth values in the study area. The best-fit lines were determined from the power spectrum curves by using the least-squares method. These best-fit lines correspond to depths of z_t and z_o (Fig. 5). Using Eq. 2, the Curie point depths (z_b) for each block were calculated from the obtained depths of z_t and z_o. The depth map of the study area was created by using the z_t, z_o and z_b values of each block (Fig. 6).

CALCULATION OF HEAT FLOW

The evaluation of variations of an area's Curie isotherm can provide valuable information about the regional temperature distribution at depth and concentration of underground geothermal energy. One of the important parameters determining the relative depth of the Curie isotherm with respect to sea level is the local thermal gradient (i.e, the heat flow and thermal conductivity structure). Measurements have shown that a region with significant geothermal energy is characterized by an abnormally high-temperature gradient and heat flow. Therefore, geothermally active areas can be expected to be associated with shallow Curie point depths (Tselentis 1991). Analyses of long-wavelength magnetic anomalies have provided valuable information about magnetization sources and Curie depth, which can offer insight into
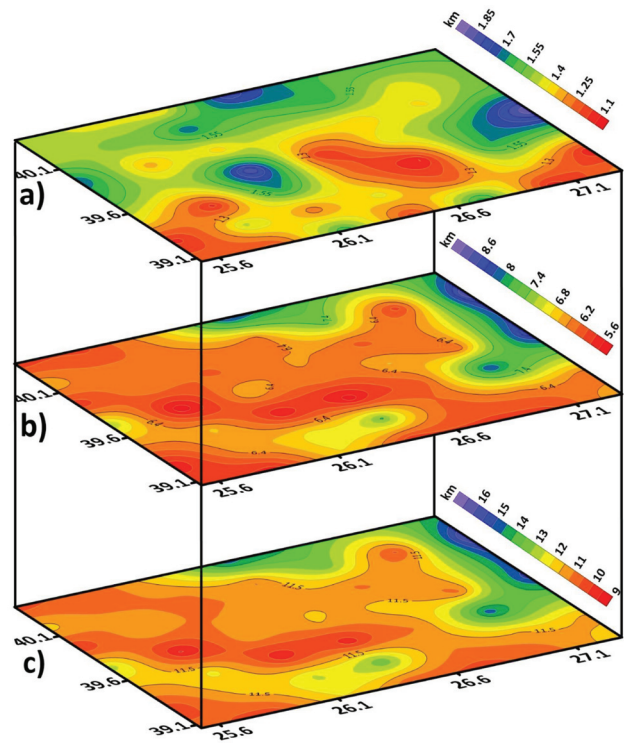
Fig. 6 Spatial distribution of the magnetized body at different depths: **a)** z_t, depth of the top of the magnetic body, **b)** z_o, depth of the middle of the magnetic body, and **c)** z_b, depth of the bottom of the magnetic body

the proxy heat flow of a region (Bansal *et al.* 2013).

Lachenbruch and Sass (1978) modelled geotherms under various conditions (extension, magmatic underplating, and intrusion) and developed formulas for the modelling process (Eq. 3 and 4). The average temperature at any z depth is defined by Eq. 3.

$$\theta(z;R,\beta,q_a) = A_0\frac{D^2}{K}\left(1-\frac{D^2}{\beta^2}\right)^{-1}\left(\frac{\cosh\frac{R-z}{\beta}}{\cosh\frac{R}{\beta}}-e^{-z/D}\right)$$
$$+\left(\theta_0+\frac{L}{c}\right)\left(1-\frac{\cosh\frac{R-z}{\beta}}{\cosh\frac{R}{\beta}}\right)$$
$$+\frac{\beta}{K}\left[q_a-A_0\frac{D^2}{\beta^2}\left(1-\frac{D^2}{\beta^2}\right)^{-1}e^{-R/D}-2mK\right]\frac{\sinh\frac{z}{\beta}}{\cosh\frac{R}{\beta}}+2mz \quad (3)$$

From Eq. 3, the heat flow at the surface ($z = 0$) is calculated as Eq. 4.

$$\theta(0;R,\beta,q_a) = A_0 D\left(1-\frac{D^2}{\beta^2}\right)^{-1}\left(1-\frac{D}{\beta}\tanh\frac{R}{\beta}\right)+$$
$$+\frac{K}{\beta}\left(\theta_0+\frac{L}{c}\right)\tanh\frac{R}{\beta}$$
$$+\left[q_a-A_0\frac{D^3}{\beta^2}\left(1-\frac{D^2}{\beta^2}\right)^{-1}e^{-R/D}-2mK\right]\frac{1}{\cosh\frac{R}{\beta}}+2mK \quad (4)$$

where
q_a is asthenospheric heat flow (mW/m²),
K is thermal conductivity (W/m/K),
A_0 is linear heat production (microW/m³),
D is the effective depth of heat production (km),
R is lithospheric thickness (km),
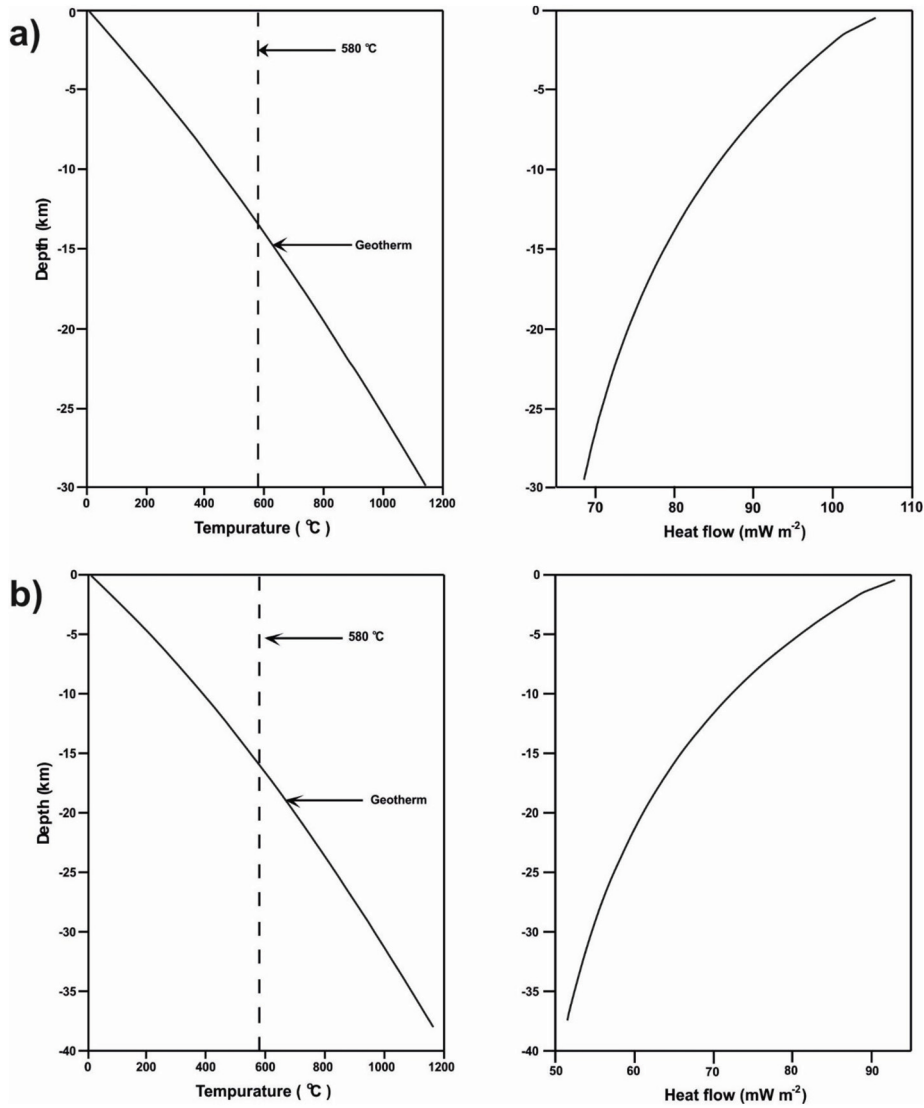
Fig. 7 Steady state geotherms (left panels) and heat flow with depth (right panels) computed using the methods of Lachenbruch and Sass (1978) to approximate the estimated conditions in the study area. Asthenospheric and reduced heat flow equal, i.e., qa = qr, strain rate of 0.75% (my)⁻¹, thermal conductivity (k) is 2.127 Wm⁻¹K⁻¹, effective depth of heat production (D) is 12.5 km, linear heat production (A₀) is 2.09 µWm⁻³. **a)** Representative Block-11, **b)** Representative Block-42

s is horizontal strain rate (1 percent/m.y.), and θ is temperature (°C).

In this study, we assumed the thermal conductivity as 2.127 Wm^{-1}K^{-1} (k), effective depth of heat production 12.5 km (D) (average focal depths of earthquakes occurring in the study area), linear heat production 2.09 μWm^{-3} (A$_o$), and horizontal strain rate 0.75% (s). One-dimensional heat flow models were obtained for 49 blocks. One dimensional heat flow model for blocks 11 and 42 is given in Fig. 7. The surface heat flow (q$_s$) values obtained for each block are mapped and shown in Fig. 8. Surface heat flow values (q$_s$) vary between 92.9 and 141.6 mWm^{-2} in the study area.

When Fig. 8 is examined, the heat flow is relatively low in areas where Palaeozoic and Precambrian units are located, because these rocks generally have low permeability and low heat conduction. Regions showing high heat flow indicate places where geothermal potential may be present. The heat flow distribution in the region is heterogeneous and there are high temperature anomaly regions at certain points. The region where Precambrian rocks is located in the eastern and north-eastern parts of the study area. In these regions, the heat flow generally varies between 100–116 mW/m². In particular, one of the lowest heat flow values (approximately 92–100 mW/m²) is observed in this area. Palaeozoic rocks are observed in the northern, northeastern and central parts of the study area. In these areas, the heat flow generally varies between 108–124 mW/m². According to Figs 1 and 8, there are some points where the heat flow is relatively higher within the Precambrian and Palaeozoic units. These regions contained small granitoic intrusions. In the western and south-western parts of the study area, the heat flow reaches 132–140 mW/m² levels. It can be said that there are no Palaeozoic or Precambrian units in these areas or that there are more permeable geological structures. In the
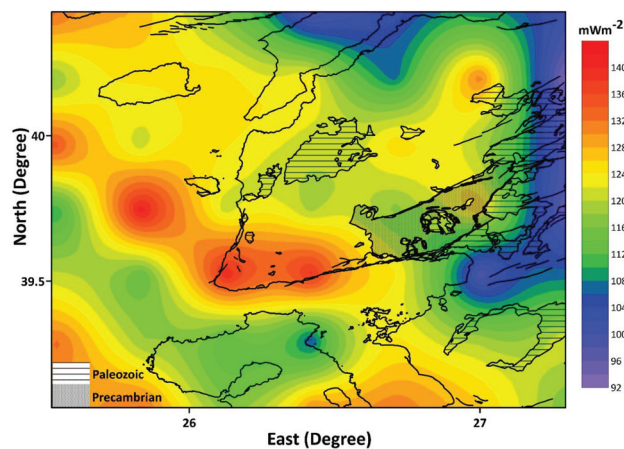
regions containing Precambrian units, the heat flow varies between 92–116 mW/m², which constitutes the lowest heat flow sections of the map. In the areas containing Palaeozoic units, the heat flow is generally between 108–124 mW/m², slightly higher than in the Precambrian areas, but lower than in the hottest regions of the study area. These low heat flow values suggest that these rocks are impermeable or have low thermal conductivity and may indicate a limited potential for geothermal systems.

MODELLING OF THE TEMPERATURE STRUCTURE OF THE CRUST INTERIOR IN THE BIGA PENINSULA

In the study area, three-dimensional (3D) heat flow and temperature distribution maps of the region were created by combining the one-dimensional heat flow models and geothermic gradient changes obtained for each block. The 3D heat flow and temperature maps are shown in Fig. 9a, b. The z$_o$ and z$_t$ values obtained from the power spectrum for 49 blocks and the 1D geothermic gradient change values calculated for each block were examined together. Fig. 10 presents a series of depth maps that illustrate the relationship between the depths obtained from power spectrum analysis and those inferred from 1-dimensional (1D) geothermic gradient models. These maps are critical for understanding the thermal structure of the subsurface and validating the consistency of different geothermal depth estimation methods.

The results indicate a strong correlation between the depth values derived from these two independent methods, suggesting the reliability of the geothermic gradient model in estimating subsurface temperatures.

As a result of this examination, it was observed that the z$_t$ depth values obtained from the power spectrum and the depth values corresponding to 80 °C in the 1D geothermal gradient graph were compatible. The z$_t$ depth and depth maps corresponding to 80 °C obtained from the power spectrum in the study area are given in Fig. 10a, b. This consistency reinforces the accuracy of using power spectrum analysis for geothermal depth estimation.

Similarly, it was observed that the z$_o$ depth values obtained from the power spectrum and the depth values corresponding to 350 °C in the 1D geothermic gradient graph were compatible. The z$_o$ depth and 350 °C depth maps obtained from the power spectrum in the study area are given in Fig. 10c, d. A strong agreement between these depth estimations suggests that the power spectrum analysis effectively captures thermal variations in the subsurface. The significance of this result lies in its potential application for geothermal resource exploration, as deeper heat flow

Fig. 8 Heat flow map of the Biga Peninsula as calculated from the Curie point depths (CPD) using Eq. (2). The Curie point temperature was set equal to 580°C, and the thermal conductivity coefficient (k) to 2.1 Wm^{-1}K^{-1}

characteristics are crucial for assessing geothermal potential. The study employs Equation 5 to estimate the z_b (Curie depth point) using the depth values z_t (80°C) and z_0 (350°C). Equation 5 emerges when the depth calculation formula z_b (Curie depth point) given in Equation 2 is taken as the depth value z_t corresponding to 80 °C obtained from the 1D geothermal gradient change graph and the depth value corresponding to 350 °C as the depth z_o.

$$z_{580°C} = 2z_{350°C} - z_{80°C} \qquad (5)$$

From the geothermal gradient change values, the depth values at 80°C and 350°C, namely z_t and z_o, were substituted in Equation 2, and $z_{580°C}$ depth values were obtained and compared with the z_b values derived from the power spectrum. When the maps shown in Fig. 10e, f are examined, it is seen that the obtained $z_b / z_{580°C}$ depth values show a very good agreement. The depth maps in Fig. 10 illustrate a high degree of consistency between depth estimations obtained from the power spectrum and those derived from the 1D geothermic gradient method. The agreement across different temperature thresholds (80°C, 350°C, and 580°C) strengthens confidence in the thermal modelling of the region. The ability to accurately determine these depth values is essential for geothermal exploration, as it helps in assessing the heat flow characteristics and potential geothermal energy resources in the study area. The successful application of Equation 5 in predicting Curie depth further confirms the robustness of the approach used in this study.

RESULTS AND DISCUSSIONS

Heat flow and geothermal gradient measurements in wells on land are usually concentrated in certain areas. There is a direct proportionality between the well depth and the heat flow values obtained. The quality and reliability of heat flow data depend on many factors. On the other hand, it is possible to calculate the Curie point depths (CPDs) by using the spectral properties of magnetic data and indirectly obtain the heat flow and geothermal gradient values. The CPD calculations were successfully applied by many researchers. In this study, CPD calculations were made using the magnetic anomalies of the Biga Peninsula located in the northwest of Türkiye, and CPD data ranging from 9 km to 17 km were obtained across the peninsula. However, the main reason for the variation of these values over such a wide range is the presence of deeper CPD values in a limited region in the east of the area. If this area is excluded, the 9–14 km range better reflects the CPD distribution character of the Biga Peninsula. This depth range, which can be considered quite shallow, becomes an acceptable and explainable value considering the average crustal thickness in this area is 27 km (Ateş *et al*. 2012). These values are also consistent with the CPD values ranging from 15 km–20 km calculated by Bilim *et al*. (2021) in the region covering the east and northeast of the study area. Considering that the CPD values were obtained at depths of 15 km to 17 km in the east of the area in this study, it is evident that the values are completely compatible. It can be seen from Fig. 8 that heat flow values range from 92.9 to 141.6 mWm^{-2}, and shallow CPD values are observed, especially in the south and southwest of the region.

When the distribution of the heat flow on the Earth is examined, different geological structures give certain heat flow values. There is a relationship between the observed heat flow values and the age of tectonic events and geological units. A striking decrease in heat flow is observed from the Cenozoic to Precambrian. Low heat flow is measured in aged rock units such as Precambrian shields ($t > 600$ Ma), while high heat flow is measured around younger folds such as those from the Cenozoic ($t < 70$ Ma) (Sclater 1972). The heat flow in the Earth is generally of radioactive origin, and radioactivity is almost equal under both
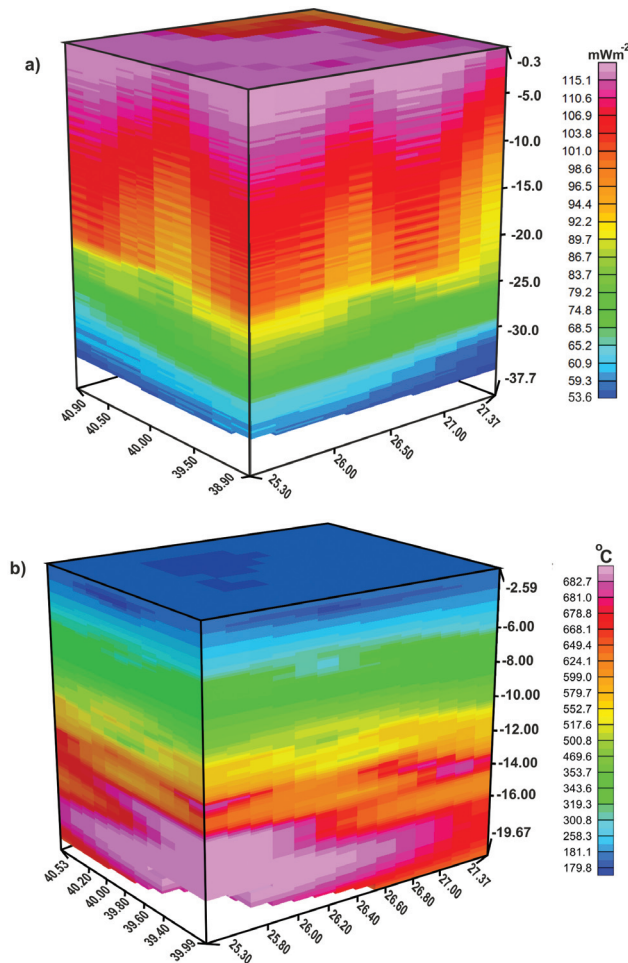
Fig. 9 3D block diagram representations: **a)** 3D heat flow and **b)** 3D temperature map of study area
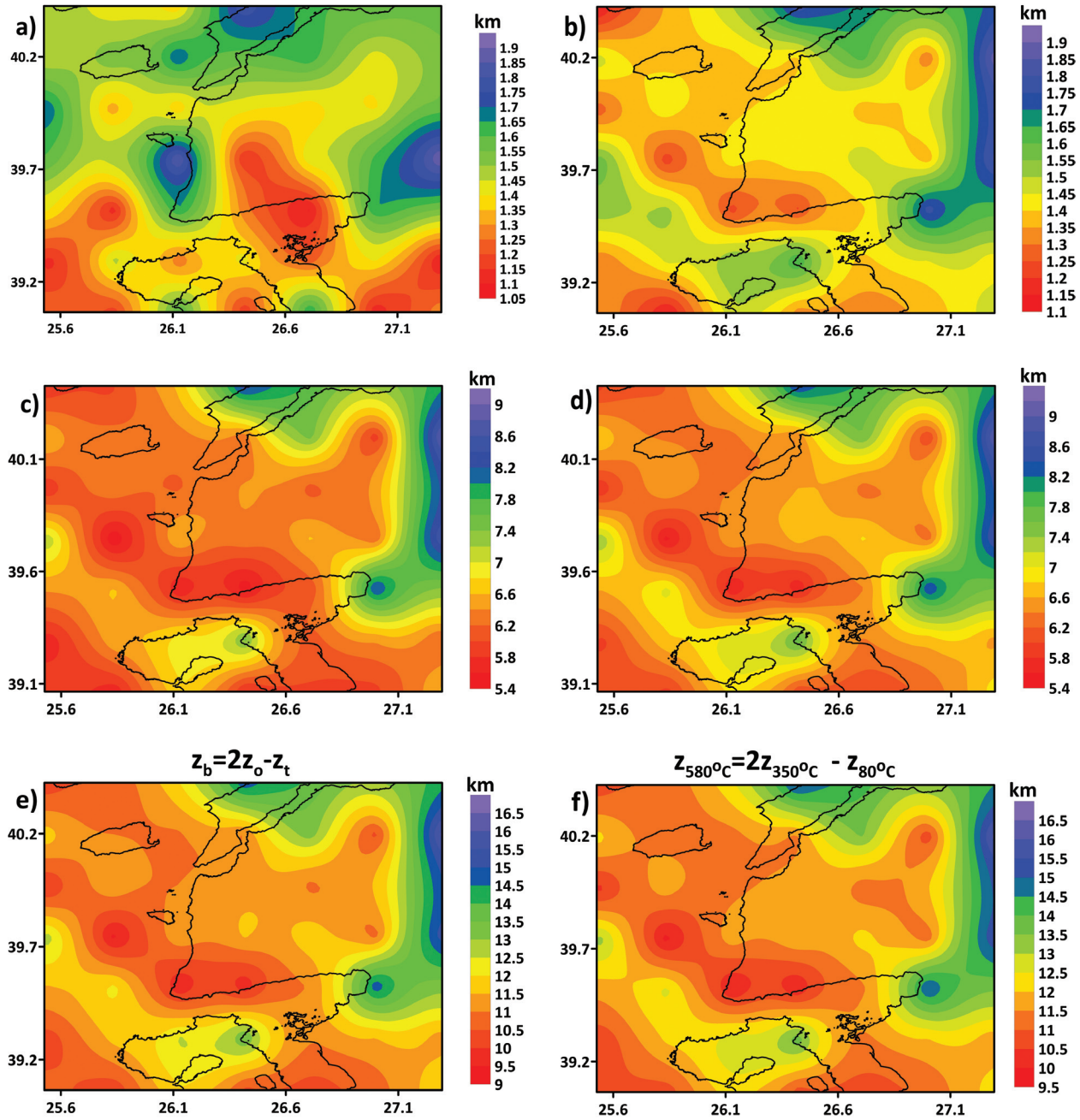
Fig. 10 a) z_t depth map obtained by power spectrum, **b)** $z_{80\,^{\circ}C}$ (depth map at 80 ℃) obtained by geothermic gradient, **c)** z_o depth map obtained by power spectrum, **d)** $z_{350\,^{\circ}C}$ (depth map at 350 ℃) obtained by geothermic gradient, **e)** z_b depth map obtained by power spectrum, **f)** z_b (Eq. 5) depth map obtained by depths at 80 ℃ and 350 ℃ ($z_{80\,^{\circ}C}$ and $z_{350\,^{\circ}C}$) using geothermic gradient

oceans and the land. However, the upper mantle is different under land and sea. When the geological structure of the Biga Peninsula is examined, the following results are observed. The Precambrian-Palaeozoic sedimentary and metamorphic rocks exhibit low heat flow values in the east and north of the area, while high heat flow values are calculated in the south and southwest, where Cenozoic granitoids and volcanic rocks crop out (Figs 1, 8).

In the calculations using the thermal models developed by Lachenbruch and Sass (1978) for such areas, variation in the temperature and heat flow values

according to the depth were obtained. When the variation of the Curie point depths calculated according to the z_t and z_o values obtained from the power spectrum calculations were compared with the heat models, it was found that each parameter corresponds to a specific heat value. Also, the z_b value, which is the CPD value, corresponds to the temperature of 580℃, the z_t value matched with 80℃, and the zo value with 350℃. According to this result, considered an important finding of this study, we suggest that z_t, z_o, and z_b depth values also correspond to certain temperature values in the upper crust. These values were obtained

25

for the Biga Peninsula, where the study was conducted, and they are too consistent to be a coincidence.

On the other hand, the Conrad discontinuity, which marks the boundary between the upper crust and the lower continental crust, where the seismic wave velocity increases discontinuously, is predicted to occur at depths of 15–20 km in various continental regions. The Conrad discontinuity depth map of Türkiye was prepared by Akın (2016) from gravity data. In this map, the Conrad discontinuity depth for the study area varies between 15–16 km. Recently, in their studies conducted by Öztürk and Alkan (2024), in which they examined the seismic and tectonic changes of Western Anatolia, it is observed that the b value is obtained around 1.0 up to 20 km in the southern part of the Biga Peninsula and increases after 20 km and reaches 1.4. Therefore, this situation has been evaluated as an important indicator that deep-rooted earthquakes will not be effective in this area. We compared the depth
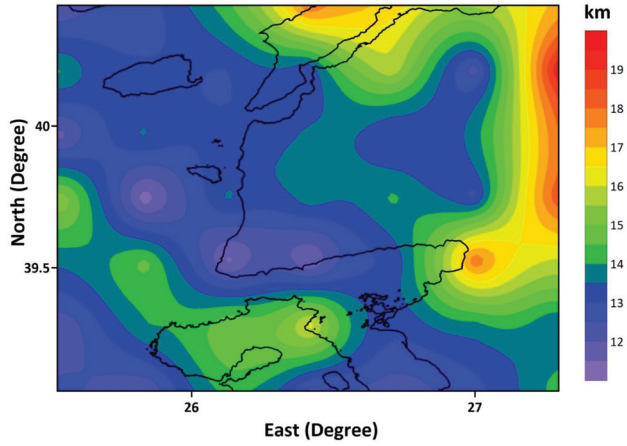
Fig. 11 Conrad depth map obtained by $z_{680\,^{o}C}$ (depth at 680 ^{o}C) using geothermic gradient
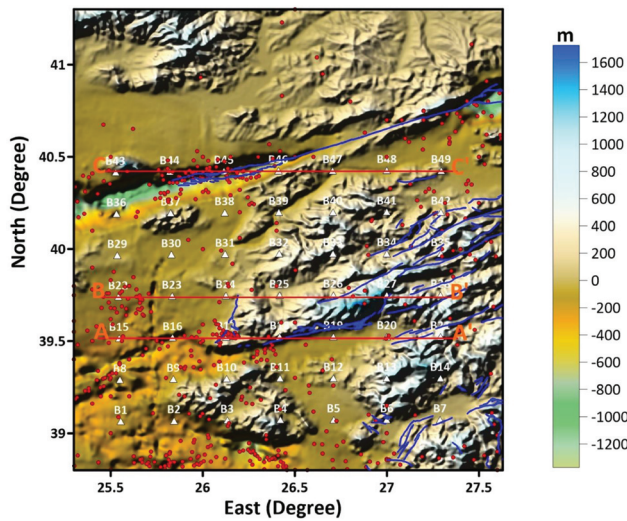
Fig. 12 Locations of two-dimensional sections of ground profiles (A–A', B–B', C–C') to describe the focal depths of earthquakes and the thermal structure of the upper crust, which varies according to depth, taking into account seismogenic zones

values corresponding to 680°C calculated from the 1D geothermal gradient changes in the study area with the Conrad discontinuity depths of Akın (2016) and defined that these are highly compatible (Fig. 11).

The z_0, which we assume as the average depth of the magnetized body in this study, corresponds to the depth where the temperature reaches 350°C. This value is accepted as the deepest rheological limit temperature value for the brittle-plastic, seismogenic rock behaviour proposed by Scholz (1990), and it represents the limit for the majority of seismic events in the upper crust. To investigate the possible relationship between the focal depths of the earthquakes and the thermal structure of the upper crust that varies with depth, sections A–A', B–B', and C–C' were taken in three different directions (taking into account the seismogenic zones) (Fig. 12), and the focal depths of earthquakes are concentrated between 350°C and 680°C (Fig. 13). Towards the north and east of the area, where the heat flow decreases and the CPD deepens, the focal depths of the earthquakes also increase and extend the range of 350°C to 680°C.

CONCLUSIONS

The Biga Peninsula in north-western Türkiye is surrounded by active faults with high seismicity. We investigated the existence of a relationship between depth-dependent thermal change, heat flow variations and the focal depths of earthquakes based on Curie point depth calculations using magnetic data.

The upper and middle depth values of the magnetized body, which are the CPD parameters (z_t, z_o) obtained from the power spectrum calculation, actually correspond to specific temperature values in the ground. Accordingly, the depth value corresponding to the temperature level of 80°C in the ground corresponds to the depth of z_t, and the depth value corresponding to the temperature level of 350°C corresponds to the depth of z_o. The temperature of the CPD, which is the average value of magnetite, the most common magnetic mineral in the earth's crust, is 580°C. Thus, the relationships can be defined as $z_t = z_{80^{o}C}$, $zo = z_{350^{o}C}$, and $z_b = z_{580^{o}C}$. CPD values vary between 9–17 km in the Biga Peninsula. Cenozoic granitoids and volcanic rocks coincide with shallower CPD depths and higher heat flow variations compared to areas where Precambrian-Palaeozoic metamorphics and sedimentary units are mapped. On the other hand, according to the heat-depth models obtained in the study, the value corresponding to the Conrad discontinuity, which ranges from 15–16 km for the Biga Peninsula, was found to be 680°C. In this case, the thermal depth equivalent of Conrad depth is given as $z_c = z_{680^{o}C}$ as a new concept. It was observed that the focal depths of the earthquakes in the Biga Peninsula
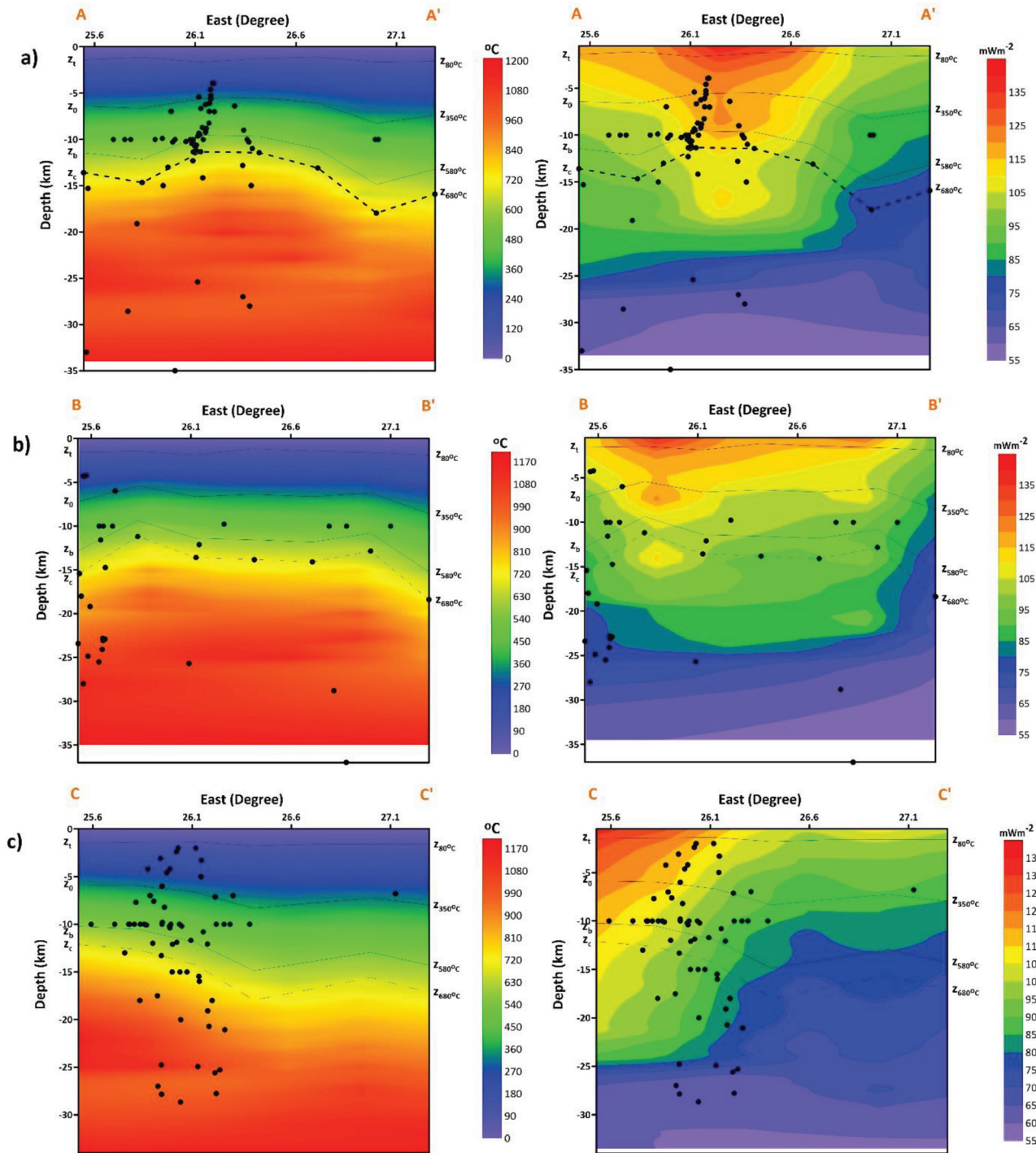
Fig. 13 2D temperature (left) and heat flow (right) sections: **a)** A–A' profile, **b)** B–B' profile, **c)** C–C' profile. The focal depths of earthquakes are concentrated between 350°C and 680°C. Towards the north and east of the area, where the heat flow decreases and the CPD deepens, the focal depths of the earthquakes also increase and extend the range of 350°C to 680°C

are concentrated depths corresponding to between 350°C and 680°C, while in the eastern regions where the heat flow decreases, they are observed below the depths corresponding to 680°C.

REFERENCES

Akbaş, B., Akdeniz, N., Aksay, A., Altun, İ.E., Balcı, V., Bilginer, E., Bilgiç, T., Duru, M., Ercan, T., Gedik, İ.,

Günay, Y., Güven, İ.H., Hakyemez, H.Y., Konak, N., Papak, İ., Pehlivan, Ş., Sevin, M., Şenel, M., Tarhan, N., Turhan, N., Türkecan, A., Ulu, Ü., Uğuz, M.F., Yurtsever, A. et al., 2011, *1:1.250.000 ölçekli Türkiye Jeoloji Haritası*. Maden Tetkik ve Arama Genel Müdürlüğü Yayını, Ankara-Türkiye.

Akbayram, K., Şengör, A.M.C., & Özcan, E. 2016. The evolution of the Intra-Pontide suture: Implications of the discovery of late Cretaceous – early Tertiary mélanges. In *Honor of Manuel Berberian's Forty-Five Years of Research Contributions: Geological Society of America, Tectonic Evolution, Collision, and Seismicity of Southwest Asia,* edited by Sorkhabi, R. *Special Paper* 525(18).

Akın, U. 2016. Investigation of the Seismic Velocity Distribution and Crustal Structure of Turkey by Means of Gravity Data. *Journal of MTA, 153*, 185–202. https://doi.org/10.19076/mta.65685

Aldanmaz, E., Pearce, J., Thirlwall, M.F., & Mitchell, J. 2000. Petrogenetic evolution of late Cenozoic, post-collision volcanism in western Anatolia. *Turkey Journal of Volcanology and Geothermal Research 102(1–2)*, 67–95. https://doi.org/10.1016/S0377-0273(00)00182-7

Altunkaynak, Ş., & Yılmaz, Y. 1999. The Kozak Pluton and its emplacement. *Geological Journal 34(3)*, 257–274. https://doi.org/10.1002/(SICI)1099-1034(199907/09)34:33.0.CO;2-Q

Altunkaynak, Ş., & Genç, Ş.C. 2008. Petrogenesis and time-progressive evolution of the Cenozoic continental volcanism in the Biga Peninsula, NW Anatolia (Turkey). *Lithos 102(1–2)*, 316–340.

Altunkaynak, Ş., Sunal, G., Aldanmaz, E., Genç, Ş.C., Dilek, Y., Furnes, H., Kenneth, A.F., Yang, J., & Yıldız, M. 2012. Eocene Granitic Magmatism in NW Anatolia (Turkey) revisited: New implications from comparative zircon SHRIMP U–Pb and 40Ar–39-Ar geochronology and isotope geochemistry on magma genesis and emplacement. *Lithos 155,* 289–309. https://doi.org/10.1016/j.lithos.2012.09.008

Altunkaynak, Ş., Dilek, Y., Genç, Ş.C., Sunal, G., Gertisser, R., Furnes, H., Foland, K.A., & Yang, Y. 2012b. Spatial, temporal and geochemical evolution of Oligo–Miocene granitoid magmatism in western Anatolia, Turkey. *Gondwana Research 21(4),* 961–986. https://doi.org/10.1016/j.gr.2011.10.010

Aslan, Z., Erdem, D., Temizel, İ., & Arslan, M. 2017. SHRIMP U-Pb zircon ages and whole-rock geochemistry for the Şapçı volcanic rocks, Biga Peninsula, Northwest Turkey: implications for pre-eruption crystallization conditions and source characteristics. *International Geology Review 59(14)*, 1764–1785. https://doi.org/10.1080/00206814.2017.1295282

Ateş, A., Bilim, F., & Büyüksaraç, A. 2005. Curie point depth investigation of Central Anatolia, Turkey. *Pure and applied Geophysics 162(2)*, 357–371. https://doi.org/10.1007/s00024-004-2605-3

Ateş, A., Bilim, F., & Büyüksaraç, A. 2012. Crustal Structure of Turkey from Aeromagnetic, Gravity and Deep Seismic Reflection Data. *Surveys in Geophysics 33*, 869–885. https://doi.org/10.1007/s10712-012-9195-x.

Ayan, M. 1979. Geochronological and petrological studies of the Eybek granodioritec pluton (Edremit). *Communication Faculty Sciences University of Ankara 22*, 19–31.

Aydemir, A., Bilim, F., Koşaroğlu, S., & Büyüksaraç, A. 2019. Thermal structure of the Cappadocia region, Turkey: a review with geophysical methods. *Mediterranean Geoscience Reviews 1*, 243–254. https://doi.org/10.1007/s42990-019-00011-7

Aydın, I., Karat, H.I., & Kocak, A. 2005. Curie-point depth map of Turkey. *Geophysical Journal International 162(2)*, 633–640. https://doi.org/10.1111/j.1365-246X.2005.02617.x

Bansal, A.R., Anand, S.P., Rajaram, M., Rao, V.K., & Dimri, V.P. 2013. Depth to the bottom of magnetic sources (DBMS) from aeromagnetic data of Central India using modified centroid method for fractal distribution of sources. *Tectonophysics 603*, 155–161.

Barka, A. 1992. The North Anatolian Fault Zone. *Annales Tectonics 6*, 164–195.

Barka, A., & Kadinsky-Cade, K. 1988. Strike-slip fault geometry in Turkey and its influence on earthquake activity. *Tectonics 7(3)*, 663–684. https://doi.org/10.1029/TC007i003p00663

Bektaş, O. 2013. Thermal structure of the crust in Inner East Anatolia from aeromagnetic and gravity data. *Physics of The Earth and Planetary Interiors 221,* 27–37. https://doi.org/10.1016/J.PEPI.2013.06.003

Bektaş, O., Ravat, D., Büyüksaraç, A., Bilim, F., & Ateş, A. 2007. Regional geothermal characterisation of East Anatolia from aeromagnetic, heat flow and gravity data. *Pure and applied Geophysics 164(5)*, 975–998. https://doi.org/10.1007/s00024-007-0196-5

Bhattacharyya, B.K., & Leu, L.K. 1975. Analysis of Magnetic Anomalies over Yellowstone National Park: Mapping and Curie Point Isothermal Surface for Geothermal Reconnaissance. *Journal of Geophysical Research 80*, 461–4465. https://doi.org/10.1029/JB080i032p04461

Bhattacharyya, B.K., & Leu, L.K. 1977. Spectral Analysis of Gravity and Magnetic Anomalies due to Rectangular Prismatic Bodies. *Geophysics 42*, 41–50. https://doi.org/10.1190/1.1440712

Bilim, F. 2011. Investigation of the Galatian volcanic complex in the northern central Turkey using potential field data. *Physics of the Earth planetary Interior 185(1–2)*, 36–43. https://doi.org/10.1016/j.pepi.2011.01.001

Bilim, F. 2017. Investigating Moho depth, Curie Point, and heat flow variations of the Yozgat Batholith and its surrounding area, north central Anatolia, Turkey, using gravity and magnetic anomalies. *Turkish Journal of Earth Sciences 26(6)*, 410–420.

Bilim, F., Akay, T., Aydemir, A., & Koşaroğlu, S. 2016. Curie point depth, heat-flow and radiogenic heat production deduced from the spectral analysis of the aeromagnetic data for geothermal investigation on the Menderes Massif and the Aegean Region, western Turkey. *Geothermics 60,* 44–57. https://doi.org/10.1016/j.geothermics.2015.12.002

Bilim, F., Koşaroğlu, S., Aydemir, A., & Büyüksaraç, A. 2017a. Thermal Investigation in the Cappadocia Region, Central Anatolia-Turkey, Analyzing Curie Point Depth, Geothermal Gradient, and Heat-Flow Maps from the Aeromagnetic Data. *Pure and Applied Geophysics 174(12)*, 4445–4458. https://doi.org/10.1007/s00024-017-1666-z

Bilim, F., Aydemir, A., & Ates, A. 2017b. Tectonics and thermal structure in the Gulf of Iskenderun (Southern Turkey) from the aeromagnetic, borehole and seismic data. *Geothermics 70*, 206–221.

Bilim, F., Aydemir, A., Ates, A. 2021. Geothermal Prospectivity of the Bigadic Basin and Surrounding Area, NW Anatolia, Turkey, by the Spectral Analysis of Magnetic Data. *Pure and Applied Geophysics 178*, 3085–3107. https://doi.org/10.1007/s00024-021-02787-y

Birkle, P., & Satır, M. 1995. Dating, geochemistry and geodynamic significance of the Tertiary magmatism of the Biga-Peninsula (Ezine, NW Turkey). In *Geology of the Black Sea region*, edited by S. Örçen, 171–180. General Directorate of Mineral Research and Exploration, Ankara.

Blakely, R.J. 1988. Curie temperature isotherm analysis and tectonic implications of aeromagnetic data from Nevada. *Journal of Geophysical Research 93(B10)*, 11817. https://doi.org/10.1029/JB093iB10p11817

Boler, F.M. 1978. Aeromagnetic measurements, magnetic source depths and Curie point isotherm in the Vale-Omyhee, Oregon. M.S. thesis, Oregon State Univ., Corvallis.

Bozkaya, G., Bozkaya, Ö., David, A.B., & Gökce, A. 2020. P-T-X constraints on the Koru epithermal base-metal (±Au) deposit, Biga Peninsula, NW Turkey. *Ore Geological Review 119*, 103349. https://doi.org/10.1016/j.oregeorev.2020.103349

Byerly, P.F. & Stolt, R.H. 1977. An attempt to define the Curie point isotherm in Northern and Central Arizona. *Geophysics* 42, 1394–1400.

Connard, G., Couch, R., & Gemperle, M. 1983. Analysis of Aeromagnetic Measurements from the Cascade Range in Central Oregon. *Geophysics 48,* 376–390. https://doi.org/10.1190/1.1441476

Çiçek, M., & Oyman, T. 2016. Origin and evolution of hydrothermal fluids in epithermal Pb-Zn-Cu ± Au ± Ag deposits at Koru and Tesbihdere mining districts, Çanakkale, Biga Peninsula, NW Turkey. *Ore Geology Reviews 78*, 176–195.

Delaloye, M., & Bingöl, E. 2000. Granitoids from western and North-western Anatolia: geochemistry and modeling of geodynamic evolution. *International Geological Review 42*, 241–268. https://doi.org/10.1080/00206810009465081

Demirel, Z., Yıldırım, T., & Burçak, M. 2004. Preliminary study on the occurrence of geothermal systems in the tectonic compressional regions: An example from the Derman geothermal field in the Biga Peninsula, Turkey. *Journal of Asian Earth Sciences 22*, 495–501. https://doi.org/10.1016/S1367-9120(03)00087-7

Deniz, O. 2010. Çanakkale Çançevresindeki jeotermal sistemlerin hidrojeolojik ve hidrojeo kimyasal incelenmesi. PhD Thesis, Dokuz Eylül University [In Turkish].

Dolmaz, M.N., Hisarli, Z.M., Ustaomer, T., & Orbay, N. 2005a. Curie point depths based on spectrum analysis of aeromagnetic data, West Anatolian extensional province, Turkey. *Pure and applied Geophysics 162(3)*, 571–590. https://doi.org/10.1007/s00024-004-2622-2

Dolmaz, M.N., Ustaomer,T., Hisarli, Z.M., & Orbay, N. 2005b. Curie point depth variations to infer thermal structure of the crust at the African Eurasian convergence zone, SW Turkey. *Earth, Planets Space 57(5)*, 373–383. https://doi.org/10.1186/BF03351821

Dolmaz, M.N., Elitok, Ö., & Kalyoncuoglu, U.Y. 2008. Interpretation of low seismicity in the Eastern Anatolian collisional zone using geophysical (seismicity and aeromagnetic) and geological data. *Pure and Applied Geophysics 165*, 311–330.

Dönmez, M., Akçay, A.E., Genç, C., & Acar, Ş. 2005. Middle–Upper Eocene volcanism and marine ignimbrites of Biga Peninsula. *Bulletin Mineral Research Exploration 131*, 49–61.

Duru, M., Pehlivan, S., Senturk, Y., Yavas, F., & Kar, H. 2004. New results on the lithostratigraphy of the Kazdag Massif in northwestern Turkey. *Turkish Journal of Earth Sciences 13*, 177–186.

Duru, M., Dönmez, M., Ilgar, A., Pehlivan, Ş., & Akçay, A.E. 2012. *Geological map of the Biga Peninsula.* Ankara: MTA (General Directorate of Mineral Research and Exploration of Turkey) Publications, scale: 1/250000.

Ekinci, Y.L., & Yiğitbaş, E. 2012. A Geophysical Approach to the Igneous Rocks in the Biga Peninsula (NW Turkey) Based on Airborne Magnetic Anomalies: Geological Implications. *Geodinamica Acta 25 (3-4)*, 267–285. https://doi.org/10.1080/09853111.2013.858945

Ekinci, Y.L., & Yiğitbaş, E. 2015. Interpretation of Gravity Anomalies to Delineate Some Structural Features of Biga and Gelibolu peninsulas, and their Surroundings (north-west Turkey). *Geodinamica Acta 27 (4)*, 300–319. https://doi.org/10.1080/09853111.2015.1046354

Elitok, O., & Dolmaz, M.N. 2008. Mantle flow-induced crustal thinning in the area between the easternmost part of the Anatolian plate and the Arabian Foreland (E Turkey) deduced from the geological and geophysical data. *Gondwana Research 13(3)*, 302–318. https://doi.org/10.1016/j.gr.2007.08.007

Emre, Ö., Duman, T., Özalp, S., Elmacı, H., Olgun, Ş., & Şaroğlu, F. 2013. Active Fault Map of Turkey with an Explanatory Text 1:1.250.000 scale. *Special Publication Series – 30*. General Directorate of Mineral Research and Exploration (MTA), Turkey.

Erbek, E., & Dolmaz, M.N. 2019. Investigation of the thermal structure and radiogenic heat production through aeromagnetic data for the southeastern Aegean Sea and western part of Turkey. *Geothermics 81,* 113–122. https://doi.org/10.1016/j.geothermics.2019.04.011

Ercan, T., & Türkecan, A. 1984. Bodrum Yarimadasijeolojisi. *MTA Dergisi 97/98*, 21–32. Ankara.

Gorgun, E., & Albora, A.M. 2017. Seismotectonic Investigation of Biga Peninsula in SW Marmara Region Using Steerable Filter Technique, Potential Field Data and Recent Seismicity. *Pure and Applied Geophysics 174(10),* 3889–3904. https://doi.org/10.1007/s00024-017-1604-0

Gülyüz, N., Gülyüz, E., Shipton, Z.K., Kuşcu, İ., & Richard, A.L. 2020. Geological and mineralization characteristics of the Kestanelik epithermal Au-Ag deposit in the Tethyan Metallogenic Belt, NW Turkey. *Geosciences Journal 24,* 407–424. https://doi.org/10.1007/s12303-019-0030-y

Harash, F. & Chen, C. 2022. Determination of Curie Point Depth Distribution and Heat Flow Regime Characteristics in Eratosthenes Seamount, Eastern Mediterranean Sea. *Energies,* 15, 8634. https://doi.org/10.3390/en15228634

Herece, E., & Akay, E. 2003. *Atlas of North Anatolian Fault (NAF). Maden Tetkik Arama Genel Müdürlüğü Özel Yayın.* Ser. 2, Ankara.

Hisarlı, Z.M. 1996. Batı Anadolu'da Curie Noktası Derinliklerinin Saptanmasıve Jeotermal Alanlarl aİlişkisi. İstanbul Üniversitesi Fen BilimleriEnstitüsü (PhD Thesis) [In Turkish].

Hisarli, Z.M., Dolmaz, M.N., Okyar, M., Etiz, A., & Orbay, N. 2012. Investigation into regional thermal structure of the Thrace Region, NWTurkey, from aeromagnetic and borehole data. *Studia Geophysisica et Geodetica 56(1),* 269–291. https://doi.org/10.1007/s11200-010-9077-y

Jankovic, S. 1986. Tethyan Eurasian Metallogenic Belt: relations of mineral associations and their tectonic setting. *Geotectonica et Metallogenia 10,* 99–124.

Jiao, L., Tu, J., Lei, Y., Zhao, J. & Wang W. 2025. Crustal magnetic structure and implications for the Eastern Himalayan Syntaxis revealed by EMAG2-v3. *Tectonophysics 896,* 230608. https://doi.org/10.1016/j.tecto.2024.230608

Karacık, Z., & Yılmaz, Y. 1998. Geology of the ignimbirites and the associated volcano plutonic complex of the Ezine area, northwestern Anatolia. *Journal of Volcanological Geothermal Research 85,* 1–4. https://doi.org/10.1016/S0377-0273(98)00058-4

Koç, G.A., Çelik, A., Demir, M.M., & Baba, A. 2015. A*şır ıtuzlujeotermalakışkanınhidrojeokimyasalözelliklerive kabukoluşumu.* III. Jeotermal Kaynaklar Sempozyumu ve Sergisi Bildiriler Kitabı p. 193. TMMOB Jeoloji Mühendisleri Odası Ankara [In Turkish].

Korfmann, M.O. 2007. *Troy: From Homer's Iliad to Hollywood epic Winkler,* edited by Martin, M., 25. Oxford, England: Blackwell Publishing Limited. ISBN 978-1-4051-3183-4

Krushensky, R.D. 1976. Neogene calc-alkalene extrusive and intrusive rocks of the Karalar-Yeşiller area, Northwest Anatolia, Turkey. *Bulletin Volcanologique 40,* 336–360. https://doi.org/10.1007/BF02597835

Lachenbruch, A.H., & Sass, J.H. 1978. Models of an extending lithosphere and heat flow in the basin and range province. In *Cenozoic Tectonics and Regional Geophysics of the Western Cordillera,* edited by Smith, R.B. and Eaton, G.P. *Geological Society of America, 152,* 209–250.

McKenzie, D.P. 1972. Active tectonics of the Mediterranean region. *Geophysical Journal Royal Astronomy Society 55,* 217–254. https://doi.org/10.1111/j.1365-246X.1972.tb02351.x

McKenzie, D.P. 1978. Active tectonics of the Alpine-Himalayan belt: the Aegean Sea and surrounding regions (tectonic of Aegean region). *Geophysical Journal Royal Astronomy Society 55,* 217–254. https://doi.org/10.1111/j.1365-246X.1978.tb04759.x

Maden, N. 2013. Geothermal structure of the eastern Black Sea basin and the eastern Pontides orogenic belt: Implications for subduction polarity of Tethys oceanic lithosphere. *Geoscience Frontiers 4 (4),* 389–398.

Maden, N. 2010. Curie-point Depth from Spectral Analysis of Magnetic Data in Erciyes Stratovolcano (Central TURKEY). *Pure and Applied Geophysics* 167, 349–358. https://doi.org/10.1007/s00024-009-0017-0

Maden, N., Gelisli, K., Eyuboglu, Y., & Bektas, O. 2009. Determination of tectonic and crustal structure of the Eastern Pontide orogenic belt (NE Turkey) using gravity and magnetic data. *Pure and Applied Geophysics 166,* 1987–2006.

Marobhe, I.M. 1989. A Versatile Turbo-Pascal Program for Optimization of Magnetic Anomalies Caused by Two-Dimensional Dike, Prism or Slope Models. *Computer & Geosciences 16,* 341–365. https://doi.org/10.1016/0098-3004(90)90068-5

Maus, S., Yin, F., Luhr, H., Manoj, C., Rother, M., Rauberg, J., Michaelis, I., Stolle, C., & Müller, R.D. 2008. Resolution of direction of oceanic magnetic lineations by the sixth-generation lithospheric magnetic field model from CHAMP satellite magnetic measurements. *Geochemistry Geophysics Geosystems 9(7),* 1–10. https://doi.org/10.1029/2008GC001949

Maus, S., Barckhausen, U., Berkenbosch, H., Bournas, N., Brozena, J., Childers, V., Dostaler, F., Fairhead, J.D., Finn, C., Von Frese, R.R.B., Gaina, C., Golynsky,S., Kucks, R., Lühr, H., Milligan, P., Mogren, S., Müller, R.D., Olesen, O., Pilkington, M., Saltus, R., Schreckenberger, B., Thébault, E., & Caratori Tontini, F. 2009. EMAG2: A 2 – arc min 57resolution Earth Magnetic Anomaly Grid compiled from satellite, airborne and marine magnetic measurements. *Geochemistry Geophysics Geosystems 10(8).* https://doi.org/10.1029/2009GC002471

Mohamed, A., & Al Deep, M. 2021. Depth to the bottom of the magnetic layer, crustal thickness, and heat flow in Africa: Inferences from gravity and magnetic data. *Journal of African Earth Sciences 179,* 104204.

Nagata, T. 1961. *Rock Magnetism.* Maruzen Company Ltd., Tokyo, 350 pp.

Njeudjang, K., Kana, J.D., Tom, A., Essi, J.M.A., Djongyang, N., & Tchinda, R. 2020. Curie point depth and heat flow deduced from spectral analysis of magnetic

data over Adamawa volcanic region (Northern Cameroon): geothermal implications. *SN Applied Sciences 2*, 1–16.

Njeudjang, K., Kanouo, B.M.D., Bouba, A., Nitcheu, M., Teikeu, W.A., Tamehe, L.S., Djongyang, N., & Nouck, P.N. 2023. Estimation of radiogenic heat production of the Adamawa region in Cameroon, Central Africa: an insight from spectral analysis of EMAG2 data. *Arabian Journal of Geosciences 16(7)*, 442.

Okay, A.I., & Tüysüz, O. 1999. Tethyan sutures of northern Turkey. *Geological Society London, Special Publication 156*, 475–515. https://doi.org/10.1144/GSL.SP.1999.156.01.22

Okay, A.I., Siyako, M., & Burkan, K.A. 1990. Geology and tectonic evolution of the Biga Peninsula. *Turkish Association Petroleum Geological Bulletin 2*, 83–121.

Okay, A.I., Siyako, M., & Burkan, K.A. 1991. Geology and tectonic evolution of the Biga Peninsula. Special Issue on Tectonics (ed. J.F. Dewey). *Bulletin of Technical University of Istanbul 44*, 191–255.

Okubo, Y., Graf, R.J., Hansen, R.O., Ogawa, K., & Tsu, H. 1985. Curie Point Depths of the Island of Kyushu and Surrounding Areas, Japan. *Geophysics 50,* 481–494. https://doi.org/10.1190/1.1441926

Okubo, Y., Tsu, H., & Ogawa, K. 1989. Estimation of Curie point temperature and geothermal structure of island arcs of Japan. *Tectonophysics 159(3–4)*, 279–290.

Öztürk, S., & Alkan, H. 2024. An Evaluation of the Earthquake Potential with Seismic and Tectonic Variables in the West Anatolian Region of Türkiye. *Baltica Journal on Geosciences 37(2)*, 110–124.

Pamuk, E. 2019. Investigating edge detection, Curie point depth, and heat flow using EMAG2 magnetic and EGM08 gravity data in the northern part of Eastern Anatolia, Turkey. *Turkish Journal of Earth Sciences 28(6)*, 805–821.

Pamuk, E., & Özsöz, İ. 2022. Estimation of Curie-point depths and heat flow from spectral analysis of EMAG2 magnetic data in Cyprus Island. *Annals of Geophysics 65(4)*, GD427–GD427.

Saatçi, E.S., & Aslan, Z. 2018. Petrography and petrology of The Yürekli (Balıkesir) volcanics: an example of post-collisional felsic volcanism in the Biga peninsula (NW Turkey). *Bulletin of Mineral Research Exploration 157*, 103–120. https://doi.org/10.19111/bulletinofmre.428294

Scholz, C.H. 1990. *The Mechanics of Earthquakes and Faulting*. Cambridge University Press.

Sclater, J.G. 1972. New perspectives in terrestrial heat flow. *Tectonophysics 13*, 257–291.

Shuey, R.T., Schellinger, D.K., Tripp, A.C., & Alley, L.B. 1977. Curie depth determination from aeromagnetic spectra.*Geophysical Journal Royal Astronomy Society 50*, 75–101.

Siyako, M., Bürkan, K.A., & Okay, A.İ. 1989. Tertiary geology and hydrocarbon potential of the Biga and Gelibolu Peninsula. *TAPG Bulletin 1*, 183–199.

Smith, R.B., Shuey, R.T., Freidline, R.O., Otis, R.M., & Alley, L.B. 1974. Yellowstone hot spot: new magnetic and seismic evidence. *Geology 2*, 451–455.

Spector, A., & Grant, F.S. 1970. Statistical Models for Interpretation Aeromagnetic Data. *Geophysics 35*, 293–302. https://doi.org/10.1190/1.1440092

Şalk, M., Pamukçu, O., & Kaftan, I. 2005. Determination of the Curie point depth and heat flow from MAGSAT data of Western Anatolia. *Journal of the Balkan Geophysical Society, 8(4)*,149–160.

Şaroğlu, F., Emre, Ö., & Kuşçu, İ. 1992. *Active fault map of Turkey*. Ankara.

Şengör, A.M.C. 1979. The North Anatolian transform fault: Its age, offset and tectonic significance. *Journal of the Geological Society [London] 136*, 269–282.

Şengör, A.M.C., & Yilmaz, Y. 1981. Tethyan evolution of Turkey: A plate tectonic approach. *Tectonophysics 75(3–4)*, 181–190. https://doi.org/10.1016/0040-1951(81)90275-4

Şengör, A.M.C., Tüysüz, O., Imren, C., Sakınç, M., Eyidoğan, H., Görür, N., Le Pichon, X., & Rangin, C. 2005. The North Anatolian fault: A new look. *Annual Review Earth Planetary Sciences 33*, 37–112.

Şengün, F., Yiğitbaş, E., & Tunç. İ.O. 2011. Geology and tectonic emplacement of eclogite and blueschist, Biga Peninsula, northwest Turkey. *Turkish Journal of Earth Sciences 20(3)*, 273–285. https://doi.org/10.3906/yer-0912-75

Taymaz, T., Jackson, J., & McKenzie, D. 1991. Active tectonics of the north and central Aegean Sea. *Geophysical Journal International 106(2)*, 433–490. https://doi.org/10.1111/j.1365-246X.1991.tb03906.x

Tselentis, G.A.1991. An Attempt to Define Curie Point Depths in Greece from Aeromagnetic and Heat Flow Data. *Pure and Applied Geophysics 136*, 87–101.

Wolkersdorfer, C., Stadler, S., Bretzler, A., Müller, C., & Zedler, C. 2021. Hydrochemical investigations to locate Homer's hot and cold springs of Troia (Troy)/Turkey. *Catena 200*, 105070. https://doi.org/10.1016/j.catena.2020.105070

Yiğit, O. 2012. A prospective sector in the Tethyan Metallogenic Belt: Geology and geochronology of mineral deposits in the Biga Peninsula NW Turkey. *Ore Geological Review 46*, 118–148. https://doi.org/10.1016/j.oregeorev.2011.09.015

Yiğitbaş, E., Şengün, F., & Tunç, I.O. 2009. Distribution and correlation of the Mesozoic rocks associations in the NW Anatolia (p. 118). *TÜBİTAK Report* (Project No; ÇAYDAG 108Y232).

Yin, Y., Li, C.F, & Lu, Y. 2021. Estimating Curie-point depths using both wavelet-based and Fourier spectral centroid methods in the western Pacific marginal seas. G*eophysical Journal International 227(2)*, 798–812.